

# HIGH-RESOLUTION RADIAL VELOCITY MAPPING OF OPTICAL FILAMENTS IN EVOLVED SUPERNOVA REMNANTS.

H. Greidanus, Sterrewacht Leiden, The Netherlands.  
R.G. Strom, Netherlands Foundation for Radio Astronomy.

Abstract: We report on observations of the kinematical structure of optical filaments in evolved supernova remnants, using an imaging Fabry-Perot interferometer. The radial velocity characteristics as seen in [OIII]  $\lambda 5007$  emission in one area in the Cygnus Loop are described, where four kinematically different components contributing to the emission can be recognized.

## 1. Introduction.

We have mapped the radial velocity distribution of the optically emitting gas in a number of 7'-sized fields in several evolved supernova remnants, using the H $\alpha$  and [OIII]  $\lambda 5007$  lines at a resolution of 1".2 x 1".2 x 8 km/s. The observations allow us to study the kinematical structure of the filaments in two dimensions. This is a considerable improvement over previous kinematical work on supernova remnants, which has been limited to one spatial dimension (slit spectra) or a number of sample points (aperture spectra; conventional Fabry-Perot). Previous work has, apart from that, mostly been concerned with global expansion properties. Here, we report briefly on the results for the [OIII] line in one field in the Cygnus Loop.

## 2. Observations.

The instrument used was TAURUS, an imaging Fabry-Perot interferometer, on the 2.5 m Isaac Newton telescope of the Roque de los Muchachos Observatory at La Palma. TAURUS is described in detail in Atherton et al. 1982; in outline, it works as follows. The ring-modulated interference pattern, obtained by putting a Fabry-Perot etalon in the collimated beam, is imaged on a two dimensional detector. This is done for a large number of consecutive etalon gap sizes, ultimately changing the gap size by somewhat more than one wavelength. Such a 'scan' produces a data cube of intensity as a function of two position coordinates (x,y) and one gap size coordinate (z). With a calibration cube obtained by observing a Neon lamp in the same way, the gap size coordinate is transformed to a wavelength coordinate, and thus to radial velocity. (In the following, all velocities refer to radial velocities.) An interference filter was used to separate the emission line of interest. The detector was an Image Photon Counting System (Boksenberg 1972), characterized by a very low readout noise; its use is indicated by the necessity to complete a scan as quickly as possible to minimize changes in atmospheric transparency. The range in velocity  $\Delta v$  is set by the free spectral range of the etalon,  $\text{fsr} = \lambda/2G = \Delta v/c$ . With a gap size G of 265  $\mu$ ,  $\Delta v=285$  km/s at  $\lambda=5007$   $\text{\AA}$ .

One possible cause of error that should be mentioned here is a change in alignment between the etalon and the detector, giving rise to a

systematic offset in velocity, with a magnitude varying linearly across the field. However, the alignment was checked during the night, and we do not expect this error to be present to any significant degree.

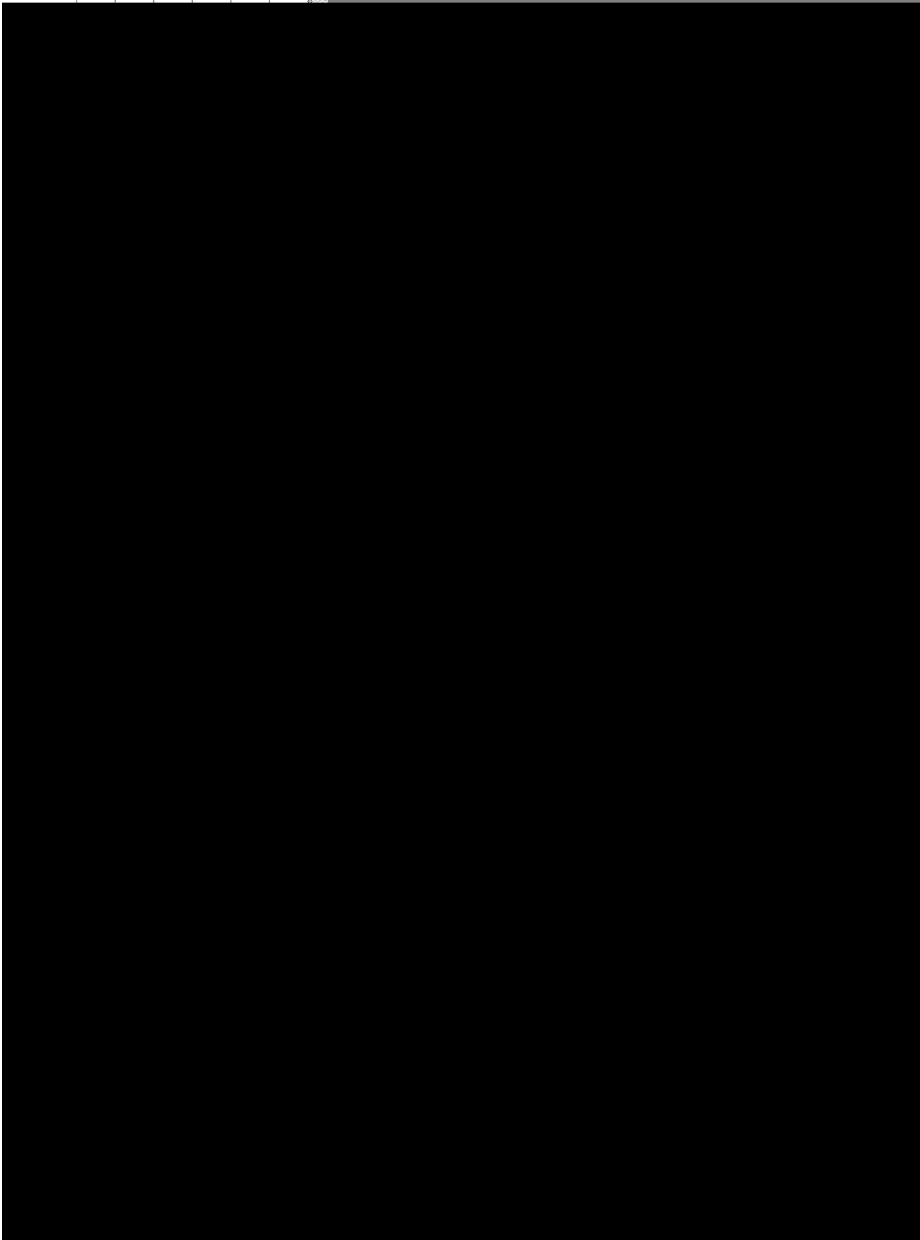
### 3. Results and discussion.

Figure 1a shows one of the observed fields, located at  $\alpha=20:46:29.1$ ,  $\delta=31^{\circ}15'07''$  (in the 'carrot', the rich filamentary area in the North-central part of the Cygnus Loop), in total [OIII]  $\lambda 5007$  intensity. Other fields in the Cygnus Loop that have been observed show kinematical properties which recur here, and we will limit the presentation to this particular field. Figures 1b and 1c show two position-velocity maps, crosscuts through figure 1a as indicated. In order to bring out the low-level emission, the data have been smoothed to  $5'' \times 5'' \times 15$  km/s. On inspecting the data cube for this field, the emission can be divided into four components, which can also be recognized in these two sample crosscuts: (1) The filaments, showing the strongest emission, narrow in one spatial dimension, generally located at moderate velocities, with (deconvolved) velocity widths of about 45 to 60 km/s; (2) The diffuse gas appearing between the filaments, linking them in a continuous way, going out to more extreme velocities, with a velocity width of the order of 35 km/s; (3) A weak component, very broad in velocity (typically about 150 km/s), present over almost the entire field and enveloping the brighter parts; (4) A weak, smooth component, very narrow in velocity ( $\sim 15$  km/s), appearing at the same central velocity throughout.

The lack of any structure in the velocity of the last component indicates that this is unaccelerated gas; because it is not found in locations where other components are weak (as in the western part of the field), it is probably not unassociated fore- or background material. Photoionized gas ahead of the shock would be a possibility. We do not have an absolute velocity calibration, but putting component 4 at  $v=0$ , most filaments appear between  $v=0$  and  $v=-80$  km/s, and only a few are seen at positive velocities up to  $v=+20$  km/s. Following individual, well-defined filaments, the velocity can be seen to change up to 20 km/s over  $\sim 1'$ . Diffuse inter-filament emission is seen up to  $v=-110$  km/s between filaments at negative velocities and up to  $v=+60$  km/s between ones at positive velocities. Apart from some low-level emission associated with component 3, which in places fills the entire spectral range, all emission is well contained within the range.

The kinematical appearance of components 1 and 2 is not inconsistent with the picture of a wrinkled sheet, the velocity characteristics being purely a projection effect, as recently modeled in Hester 1987. On the other hand, translating velocity into density, there must exist a density distribution which, when hit by a shock, gives rise to the observed velocity distribution; at least in the case where velocity is a single-valued function of position, as seen for example in figure 1c at A. This leads to the picture of pre-existing rope-like filaments with not-too-steep radial density profiles. However, a velocity profile which is a continuous, double valued function of position, as seen in figure 1b at B, cannot be interpreted in this way, but is more naturally explained as the edge of an expanding bubble. In any case, the notion that the gas at negative velocities is situated at the front side of the remnant, and the gas at positive velocities at the rear side seems obvious. But there are

**Fig. 1a.** [OIII]  $\lambda 5007$  emission of a field in the Cygnus Loop, centered at  $\alpha=20:46:29.1$ ,  $\delta=31^{\circ}15'07''$ . The grayscale has a logarithmic increment, while the contoursteps are linear.



**Fig. 1b,c.** Position-velocity crosscuts through figure 1a as indicated. Intensity in the 5007 line is plotted as a function of right ascension (this axis is the same as in figure 1a) and radial velocity. The grayscale has a linear increment, as do the contours but with a stepsize 2.5 times larger. Note the stars which appear as vertical bars.

some places where the emission is seen to go continuously from positive to negative velocities, complicating that idea, as this field is not near the remnant's edge.

#### 4. Future work.

This contribution reports on the status of our work at the time of the conference, and is not intended to be the final word. For one thing, the very limited interpretation given here for the filament/diffuse gas components 1 and 2, has only considered velocities; a following step will be to check whether both velocities and intensities are consistent with the sheet picture or the pre-existing filament picture. Furthermore, the kinematics of the H $\alpha$ -emitting gas will have to be analysed and included in the interpretation.

Observations at sub-arcsecond resolution would be interesting, to check if the velocity width in components 1 and 2, which is still considerably above the expected thermal velocity dispersion for oxygen of 12 km/s, would decrease with greater spatial resolution. Finally, to confirm the photoionized nature of component 4, this type of observation should be repeated at other wavelengths, to obtain line-ratios for this component.

#### References.

- Atherton et al. 1982, M.N.R.A.S. 201, 661.  
Boksenberg 1972, Auxiliary Instrumentation for Large Telescopes,  
Proc. of ESO/CERN Conf. Geneva, p.205.  
Hester 1987, Astroph. J. 314, 187.